

## Enhancement of pool boiling heat transfer by surface micro-structuring

This article has been downloaded from IOPscience. Please scroll down to see the full text article.

2012 J. Phys.: Conf. Ser. 395 012175

(<http://iopscience.iop.org/1742-6596/395/1/012175>)

View [the table of contents for this issue](#), or go to the [journal homepage](#) for more

Download details:

IP Address: 193.136.142.145

The article was downloaded on 30/11/2012 at 16:31

Please note that [terms and conditions apply](#).

# Enhancement of pool boiling heat transfer by surface micro-structuring

A S Moita<sup>1</sup>, E Teodori<sup>1</sup> and A L N Moreira<sup>1</sup>

Instituto Superior Técnico – TU Lisbon, Lisbon, Portugal

E-mail: [anamoita@dem.ist.utl.pt](mailto:anamoita@dem.ist.utl.pt)

**Abstract.** The present paper addresses the use of surfaces structured with arrays of square micro-cavities to enhance pool boiling heat transfer. The heat transfer performance, obtained with the structured surfaces is evaluated based on the measured boiling curves and on the heat transfer coefficients. Two new parameters are suggested to relate the bubble dynamics (and consequently the surface topography) with the heat transfer coefficients: the modified dimensionless cavity spacing and the dimensionless distance, which cover the governing parameters of the phenomena. Correlations of these parameters with the heat transfer coefficients allowed to identify the best performing patterns, from those tested so far. Based on this progress it is expected that optimization of these relations will lead to precise relations which allow a systematic optimization of the surface pattern leading to an effective heat transfer enhancement, for situations involving high heat fluxes.

## 1. Introduction

Effectiveness and hardware simplicity turn pool boiling in an attractive approach for cooling applications, particularly in high energy density systems, such as nuclear reactor power plants and electronic devices. Its effectiveness is due to the particular mechanism of heat transfer which involves three parcels, namely the natural convection from the heating surface to the fluid, the bulk convection induced by bubble growing and detachment and the vapour convection directly transferred into the bubble from the surface [1]. These parcels are influenced by several variables such as the bubble size, the departure frequency, the nucleation sites density, the thermo physical properties of the fluids and the surface topography, among others. So, one may stand that the heat transfer coefficient is a complex function of these variables. One of the variables which is easier to alter in a systematic way is the surface topography, which is known to increase the liquid/solid contact area and promote the appearance of active nucleation sites within the heterogeneous nucleation process [2]. While the first is an obvious benefit, the latter is not so straightforward. Indeed, a larger number of active nucleation sites should promote the bulk convection induced by bubble detachment and the vapour convection, but it also promotes several interaction mechanisms between nucleation sites, which may enhance or actually inhibit it, so that the negative effects of such interaction can overcome the potential advantages. These interactions are particularly intense at high heat fluxes, which are the main target in the cooling of high energy density systems. The interaction phenomena caught the attention of pioneering researchers, such as [3] and more recently [4]. The relation between the dimensionless cavity spacing  $S/\overline{D}_b$  - i.e. the ratio of the cavity spacing to the average bubble departure diameter, and the average bubble departure frequency  $\overline{f}_b$  were the parameters used to identify the different interaction regions. In the abovementioned studies, the authors tried to define interaction regions, as a

function of  $S/\overline{D}_b$ . However, each author established different regions. The most unifying theory was proposed by [4] who associated the interaction regions, also as a function of  $S/\overline{D}_b$ , with the relative importance of three competitive effects, namely the hydrodynamic interaction between bubbles, the thermal interaction between nucleation sites and the horizontal and declining bubble coalescence. The main limitation of this study is the very restricted number of cavities which turns difficult any extrapolation to the rough surfaces used in practical applications, which have numerous cavities. In this context, the present work stands for the use of various micro-cavities. Recent studies, based on a limited number of micro-cavities (e.g. [5, 6]) allowed to relate the decline of the heat transfer coefficient observed at high heat fluxes (but still away from the Critical Heat Flux conditions) with the formation of large vapour bubbles, induced by the occurrence of horizontal coalescence among nucleation sites. These large bubbles cover the surface causing the decline the heat transfer, due to the low thermal conductivity of vapour and to the fact that they reduce the induced liquid motion. This suggests that especially for higher heat fluxes, an optimal pattern of the structural elements can be obtained, which besides augmenting the liquid/solid contact area, keeps the inhibitive interaction among nucleation sites under acceptable intensity, thus ensuring an overall improved cooling performance. This may be so, since recent work, [7] suggests the establishment of an optimum inter-cavity spacing, for which most of the surface remains active for a wide range of heat fluxes, although the authors are not very clear on the arguments sustaining this optimum spacing.

In this context, the present work addresses a detailed study on the pool boiling processes on surfaces with a known and well defined number of artificially created cavities, to quantify the effect of the surface topography, on the interaction mechanisms, and particularly on the horizontal coalescence. Bubble dynamics is investigated as a function of the distance among cavities and is then correlated to the heat transfer coefficients.

## 2. Experimental setup

### 2.1. Experimental arrangement

The experimental arrangement mainly consists on a power supply, a heating block, a pool boiling test section, a high-speed camera (Phantom v4.2 from Vision Research Inc., with 512x512pixels@2100fps and a maximum frame rate of 90kfps) and a temperature acquisition system. Backlight illumination is provided by a 450W LED spotlight, passing through a diffusing glass to homogenize the background light. Type-K thermocouples are used to monitor and acquire the temperature and evaluate the heat flux. The signals of the thermocouples are sampled with a National Instruments DAQ board plus a BNC2120 and amplified with a gain of 300 before processing. The acquisition frequency is 100Hz and the temperature is monitored for 20 seconds after reaching a stable condition of the system that in this case has been represented by a constant temperature variation of  $\pm 0.5^\circ\text{C}$ . The heating module consists on a copper support, insulated by fibreglass and heated by two electric cartridge heaters. The temperature distribution of the copper support has been evaluated by mean of temperature measurements with a range of imposed heat flux. The heat losses evaluated for this configuration are 37% in the worst case. The micro-textured surfaces are placed on the top of the copper support. These surfaces, which have an area of  $1\text{cm}^2$ , are made from silicon wafers with a thickness of  $380\ \mu\text{m}$ . The boiling section is directly built over the copper support. It has an area of  $7.05\text{cm}^2$  and a height of 15mm. The amount of liquid is 7ml. Additional information is reported in [8].

## 2.2. Characterization of micro-textured surfaces

From the numerous patterns which were custom made to determine the effect of the surface topography in the boiling mechanisms, the surfaces used in this study were micro-textured with square cavities.

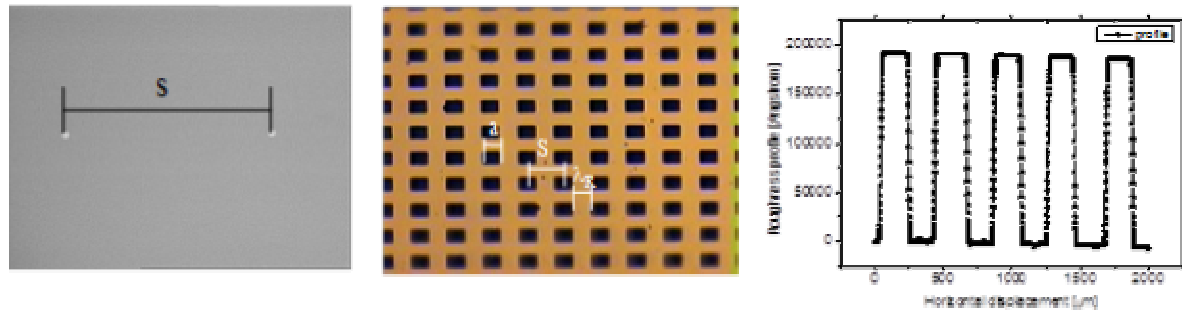


**Figure 1.** Detail of a micro-textured surface, showing the definition of the dimensions  $a$ ,  $h_r$ ,  $\lambda_R$  and  $S$  characterizing its topography.

**Table 1.** Summary of the main range of the topographical characteristics used in the customized micro-textured surfaces.  $N_{cav}$  is the number of cavities in the entire surface.

Material	Reference	$a$ [ $\mu\text{m}$ ]	$h_r$ [ $\mu\text{m}$ ]	$S$ [ $\mu\text{m}$ ]	$\lambda_R$ [ $\mu\text{m}$ ]	$N_{cav}$
Silicon	Smooth	$\approx 0$	$\approx 0$	$\approx 0$	$\approx 0$	$\approx 0$
Wafer	C1	204	30	464	260	441
	C2	286	30	626	340	256
	C3	127	30	304	177	1089
	C4	52	20	400	452	625
	C5	52	20	700	752	196
	C6	52	20	800	852	144
	C7	52	20	1200	1252	64

The patterns are custom made, combining wet etching with plasma etching. The size and depth of the cavities was fixed for this part of the study. So, the length of the squares is  $20 \mu\text{m}$  and the depth of the cavities is  $30 \mu\text{m}$ . The distance between the centers of the cavities  $S$ , is the variable and ranges between  $200 \mu\text{m} < S < 2000 \mu\text{m}$ . These quantities, which are defined in Figure 1, are measured directly from the roughness profiles, obtained using a mechanical profile meter, with a measurement precision of  $\pm 100 \text{Angstroms}$ . The main topographical characteristics of the surfaces used here are summarized in Table 1.

## 2.3. Methodology.

The pool boiling is investigated for different liquids, namely ethanol and water, to account for the liquid properties as well as to infer on the additional effects of wettability in the observed phenomena. Qualitative and quantitative characterization of the various pool boiling regimes is achieved by combining high-speed visualization with temperature measurements and heat transfer calculations. Heat flux and heat transfer coefficients are determined for the various liquid/surface pairs. Afterwards, they are related to the bubble dynamics, which is quantified by the bubble departure diameter and frequency and active nucleation sites density.

Each boiling curve presented for every pair liquid-surface used here is averaged from seven experimental curves. The curves are obtained by varying the imposed heat flux in steps of  $15 \text{W}/\text{cm}^2$ . The temperature measurements are taken for each heat flux step when the system is considered to

attain equilibrium, i.e. when the temperature oscillation is  $\pm 0.5$  °C. Before each experiment the fluid is degassed by maintaining it in the pool at 20°C above the saturation temperature. The temperature measures have an uncertainty of  $\pm 1$ °C. The relative error associated with the determination of the heat transfer is 5%. The bubble nucleation parameters considered here are the bubble departure diameter, the bubble departure frequency and the active nucleation sites density. These parameters are quantified based on post-processing of the images recorded at 2200fps and with spatial resolution is  $9.346\mu\text{m}/\text{pixel}$ . Detailed description of the measurement procedures is presented in [8].

### 3. Results

#### 3.1. Relation between bubble nucleation and heat transfer coefficient

The interaction among nucleation sites and particularly the horizontal coalescence alters significantly the heat transfer process and consequently the heat transfer coefficients in the pool boiling. Hence the dynamics of bubble nucleation and how it is affected by surface topography must be considered in order to design surface micro-patterns capable of an effective enhancement of the pool boiling heat transfer. The region of interest lays in the working conditions for which the imposed flux is close to the critical heat flux (CHF) of the pool. This is obvious, since in most cooling applications (for instance of electronic components) the system to cool can be damaged if the imposed heat flux overcomes the CHF. Thus, in this range a very precise control of the heat transfer must be achieved, for which the surface topography plays a vital role. Detailed qualitative analysis of the boiling morphology was performed in previous work [6, 8] and suggests stronger coalescence occurring on the pool boiling of the liquid with larger surface tension, which easily leads to the formation of large vapour bubbles, resulting in the deterioration of the heat transfer coefficient. To quantify how strong is the horizontal coalescence among nucleation sites one proposes here to use a new parameter, the coalescence factor  $D^* = D_b/D_{nc}$ , defined by the ratio between the average bubble departure diameter (including coalescence) and the single diameter of the bubbles which exit the cavity with no coalescence.  $D^*$  increases with the heat flux as well as with the occurrence of horizontal coalescence.  $D^*=1$  means that there is no coalescence among nucleation sites. Figure 2(a) reports the coalescence factor versus the heat flux for water. There is a strong coalescence effect for the boiling of water over all the surfaces tested, as confirmed by the high values of  $D^*$ , always larger than 1. Pattern C3, which has the smallest distance between cavities,  $S$  and therefore the largest number of cavities is clearly promoting horizontal coalescence, so that very high values of  $D^*$  are obtained for relatively low imposed heat fluxes. Instead, patterns with larger  $S$ , between  $600\mu\text{m}$  and  $800\mu\text{m}$  delay the coalescence, allowing to reach higher imposed heat fluxes, before large values of  $D^*$  are observed. It is worth noting that pattern C4, with  $S=400\mu\text{m}$  promotes a boiling behaviour similar to that of patterns with much higher distances between cavities (between  $600\mu\text{m}$  and  $800\mu\text{m}$ ), suggesting that one can decrease  $S$  to a safe value, without endorsing too much intense coalesce. This value depends on the wetting properties and on the surface tension, since the so called well wetting liquids, with low surface tension, generate a much homogeneous pool boiling nucleation, with smaller bubbles departing from the surface. So, the effect of coalescence is less evident with ethanol (Figure 2b), since for the patterns tested here,  $D^*$  is close to one, except for very high heat fluxes. Hence, one may argue that in this case the distance between cavities can be further reduced for values bellow  $300\mu\text{m}$ .

This analysis shows that having a relation linking the distance between cavities and the promotion of coalescence is useful but is not enough to identify the critical condition for which the horizontal coalescence will deteriorate the heat transfer. This requires to establish relation between the surface pattern (in the present case, the only variable is  $S$ ) and the heat transfer coefficients. This relation is not trivial because it deals with competing effects: on one hand, decreasing  $S$  endorses horizontal coalescence, but also other interaction mechanisms as identified in [4], which will enhance the frequency of bubble departure. On the other hand decreasing  $S$  will promote larger number of potential nucleation sites which is positive for the enhancement of the heat transfer [1]. Hence, the distance between cavities  $S$  must be weighted by the coalescence factor and by the density of active nucleation

sites, giving rise to the modified dimensionless cavity spacing, proposed in the present paper  $S' = S(N_{cav} / N_{ACT}) / D_b$ , where  $S$  is the distance between cavities' centres,  $N_{CAV}$  is the cavities density on the surface,  $N_{ACT}$  is the active nucleation sites density and  $D_b$  is bubble departure diameter. The heat transfer coefficient is directly related to this frequency via the departure velocity, since  $h \propto Re^a Pr^b$ , where  $Re$  and  $Pr$  are the Reynolds and the Prandtl numbers, respectively. So, one must look at the evolution of both  $h$  and frequency  $f_d$  and find the  $S'$  which maximizes  $h$ .

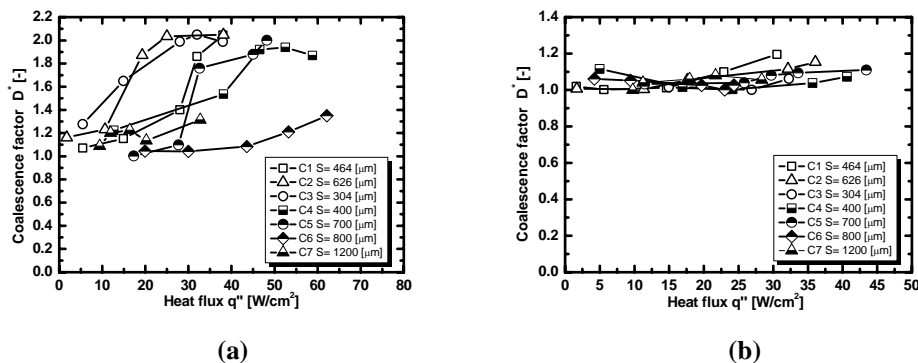


**Figure 2.** Coalescence factor versus heat flux for: (a) water (b) ethanol.

In line with this argument, Figure 3 depicts the bubble departure frequency and the heat transfer coefficient as a function of the modified dimensionless cavity spacing,  $S'$ .

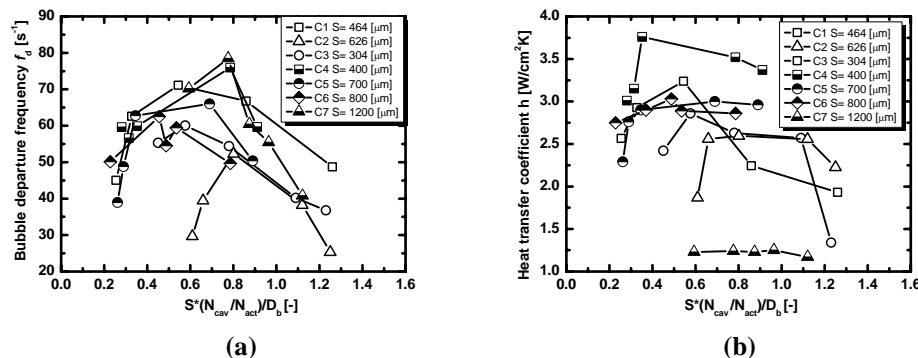


**Figure 3.** Evaluation of the interaction among nucleation sites for water: (a) Bubble departure frequency versus the modified dimensionless cavity spacing; (b) Heat transfer coefficient versus modified dimensionless cavity spacing.

The distance among nucleation sites is actually the distance among cavities only when 100% of them are active. Otherwise a homogeneous distribution of the active nucleation sites is assumed. This assumption is valid for high heat fluxes, which are the main focus of the present paper. Further research is now required to adequate this parameter with a modified distribution of  $N_{CAV}/N_{ACT}$ , for lower imposed heat fluxes, which is out of the scope of this paper. The probabilistic distribution of the active nucleation sites for a variable range of low heat fluxes is quite complex and only recently a few studies started to focus on this topic *e.g.* [9]. Focusing on the departure frequency,  $f_d$  one may indeed identify a maximum for all the surfaces tested:  $f_d$  increases with the imposed heat flux, as more nucleation sites are activated. Such trend will proceed until the maximum, after which the effect of the horizontal coalescence becomes dominant and the frequency rapidly decreases, as one tries to further increase the imposed heat flux. The highest maximum for the frequency is obtained with the patterns C1 and C4 (respectively  $S=464 \mu\text{m}$  and  $S=400 \mu\text{m}$ ) and for the pattern C7 ( $S=1200 \mu\text{m}$ ). Since the frequency is very affected by the coalescence, the patterns close to the critical condition leading to a relatively controlled increase of  $D^*$  (C1 and C4) will lead to the highest departure frequency. On the

other hand, the pattern C7, with such large  $S$  will surely preclude the occurrence of coalescence, allowing the frequency to increase up to very high imposed heat fluxes. Given that the frequency is related to the velocity of the departure bubbles, a similar trend is observed for  $h$ , although important differences are noticed, due to the effect of nucleation sites density, which will strongly influence  $h$ . Hence, looking at Figure 3b), the highest maxima occur again for the patterns C1 and C4, for which the distance between cavities is of the order of  $400\mu\text{m}$ . However, now, the effect of the nucleation sites density, weighted in the proposed dimensionless cavity spacing  $S'$  is evident and the surface C7, having very low number of cavities and therefore of active nucleation sites, gives rise to the lowest value of  $h$ . Consistently with this analysis, the boiling curves and global heat transfer coefficients depicted in Figure 4 confirm the overall best performances for the patterns C1 and C4. Also in agreement with this analysis, the curves resulting from the boiling over the pattern C7 are very close to those obtained for the smooth surface.

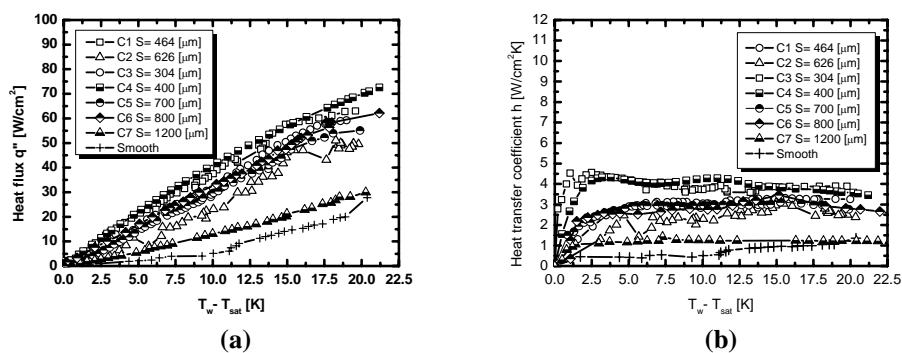


**Figure 4.** Water boiling curves on structured surfaces: (a) heat flux versus wall superheat (b) heat transfer coefficient versus wall superheat.

One may also notice that decreasing  $S'$ , by augmenting the imposed heat transfer will favour the convection due to a higher departure frequency. For the range of surfaces studied here, a maximum occurs in all of them for  $0.46 < S' < 0.78$ . Afterwards, the steep descent of both bubble frequency and  $h$  is related to the horizontal coalescence leading to the formation of a vapour blanket which insulates the surface and precludes the fluid circulation.

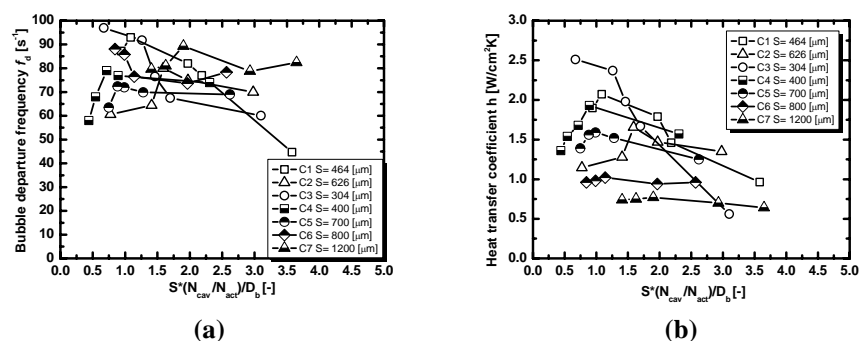


**Figure 5.** Evaluation of the interaction among nucleation sites for ethanol: (a) Bubble departure frequency versus  $S'$ ; (b) Heat transfer coefficient versus  $S'$ .

The discussion presented up to now addresses only the liquid with the highest surface tension, for which the effect of the horizontal coalescence is more evident. A similar analysis is now required to the pool boiling of the liquid with the smallest surface tension. Hence, Figure 5 depicts the departure frequency and the heat transfer coefficient obtained for the boiling of ethanol over various structured surfaces, as a function of the modified cavity spacing  $S'$ . Since for comparison purposes the same patterns are used with both liquids, the effect of the pattern is now less evident because the distance  $S$  is still quite large, so that a strong horizontal coalescence does not occur. Consequently, in Figures 5a)

and b) any maximum is detected, and the curves for the pattern with the largest  $S$  are almost constant, as this is closest to a smooth surface.

The frequency shows a trend of increasing for rising values of the heat flux (in the direction of smaller values of  $S'$ ), because the distance between the cavities is not yet small enough to be compared to the size of the bubbles. This is particularly evident for the pattern with the smallest  $S$ , (surface C3) which leads to a significant boost of the frequency (and of the heat transfer coefficient) for quite small values of the modified dimensionless cavity spacing, which are associated to higher heat fluxes.

In summary, the modified dimensionless parameter  $S'$  seems to provide useful information on the optimum distance between cavities, addressing different competitive effects which influence the overall heat transfer coefficient  $h$ . Maps of  $h$  versus  $S'$  allow to identify the surface patterns leading to a maximum value after which the heat transfer coefficient starts to deteriorate. This maximum can be easily related to the absolute distance between cavities  $S$ . However,  $S'$  does not fully address the characteristic lengths associated to the liquid properties and particularly to the surface tension. This can be accomplished using the characteristic length scale  $L_c$  from Fritz's equation [10],  $L_c = (\sigma_{lv}/g(\rho_l - \rho_v))^{1/2}$ , where  $g$  is the gravitational constant and  $\rho_l$  and  $\rho_v$  are the liquid and vapor specific masses, respectively. Figure 6 depicts the ratio between the average heat transfer coefficient of structured surfaces and that of the smooth surfaces  $h_{av}/h_{smooth}$ , versus the dimensionless distance  $S/L_c$ .

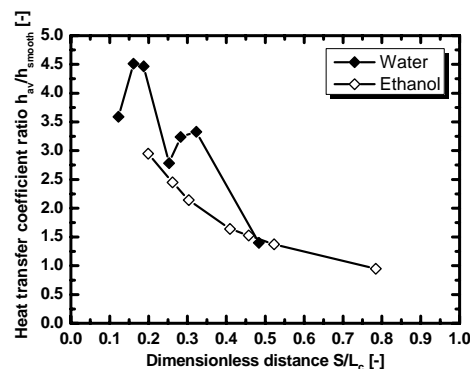


**Figure 6.** Heat transfer ratio versus dimensionless distance for water and ethanol in the range of patterns studied.

While  $h_{av}/h_{smooth}$  quantifies the potential augmentation of heat transfer coefficient obtained with the structured surface, using the smooth surface as a reference, the dimensionless distance allows relating the heat transfer coefficient with the pattern geometry (in this case with the distance between cavities), including the effect of liquid properties.  $S/L_c$  can be considered as the best dimensionless parameter to provide some guidelines on the pattern to use, as it gathers all the governing parameters. By including the properties of the liquid Figure 6 allows establishing a map of cooling performances for a wide range of pairs liquid surface. Then,  $S'$  gives additional information. For the fluid with the lowest surface tension (ethanol), the map is not well established yet as we have not reached the ranges of the patterns required to achieve a maximum. However, for water, one can identify two peaks: the maximum occurring at  $0.15 < S/L_c < 0.18$  and a lower one identified at  $0.31 < S/L_c < 0.37$ . The highest peak corresponds to the patterns with the  $S$  around  $400\mu\text{m}$ , while the second corresponds to  $S$  between  $700$  and  $800\mu\text{m}$ . The analysis based on the evolution of  $h$  as a function of  $S'$  confirms the best performance for  $S$  around  $400\mu\text{m}$ . However, if one wants to work at a safer range, since after this peak is the optimum taking advantage of limiting conditions, after which the deterioration of the  $h$  is significant, a second alternative is provided (the second peak). This is still a preliminary study so that a wider range of pairs liquid-surface is now required to confirm the utility of the plot in Figure 6.

#### 4. Final remarks

The present paper focuses on the enhancement of the heat transfer using micro-textured surfaces with arrays of a well defined number of square micro-cavities. Bubble dynamics is investigated as a



function of the distance among cavities and is then correlated to the boiling curves and to the heat transfer coefficients. Interaction among nucleation sites is quantitatively described using a new parameter, the coalescence factor  $D^* = D_b/D_{nc}$ , defined by the ratio between the average bubble departure diameter (including coalescence) and the single diameter of the bubbles which exit the cavity with no coalescence. The results indicate that, for high heat fluxes, achieving high heat transfer coefficients is a compromise between increasing the density of active nucleation sites, (thus promoting the induced convection) and controlling the interaction mechanisms, namely the horizontal coalescence, which may lead to the formation of large vapor bubbles, which deteriorate the heat transfer coefficient. The role of the horizontal coalescence is particularly relevant in the pool boiling of liquids with large surface tension, such as water. Under these conditions, the heat transfer coefficients can be well related with two dimensionless parameters, namely the modified dimensionless cavity spacing  $S' = S(N_{cav}/N_{ACT})/D_b$  and the dimensionless parameter  $S/L_c$ , which account for the governing parameters relevant for the deterioration of the heat transfer coefficient at high heat fluxes. This is yet a preliminary study but correlations of these parameters with the heat transfer coefficients allowed to identify the best performing patterns, from those tested so far. Based on this progress it is expected that optimization of these relations will lead to precise relations which allow a systematic optimization of the surface pattern leading to an effective heat transfer enhancement, for situations involving high heat fluxes.

### Acknowledgements

The authors are grateful to Fundação para a Ciência e a Tecnologia (FCT) for partially financing the research under the framework of project PTDC/EME-MFE/109933/2009 and for supporting E. Teodori with a research grant. A.S. Moita also acknowledges the contribution of FCT by supporting her with a Fellowship (Ref.:SFRH/BPD/63788/2009).

### References

- [1] Han C Y, Griffith P, The mechanism of heat transfer in nucleate boiling, *Technical Report No 7673-19*, Dep. Mech. Eng., M.I.T., 1962.
- [2] Corty C, Foust A S, Surface variables inn nucleate boiling, *Chem.Eng.Progress.Symo Ser.* 51(17)1-12,1955.
- [3] Calka A and Judd R L, Some aspects of interaction among nucleation sites, *J. Heat Transfer – Transactions of the ASME*, 102(3) 461-464,1985.
- [4] Zhang L, Shoji M, Nucleation sites interaction in pool boiling on the artificial surface, *Int. J. Heat Mass Transfer*, 46(3)513-522, 2003.
- [5] McHale J P, Garimella S V, Bubble nucleation characteristics in pool boiling of wetting liquid on smooth and rough surfaces, *Int. J. Multiphase Flow*, 36 249-260, 2010.
- [6] Moita A S, Teodori E, Moreira A L N, Influence of surface topography and wettability in the boiling mechanisms, *ILASS 24th Annual Conference on Liquid Atomization and Spray Systems – ILASS2011*, Estoril, Portugal. 2011.
- [7] Nimkar D N, Bhavnani S H, Jaeger R C, Effect of nucleation sites spacing on the pool boiling characteristics of a structured surface, *Int. J. Heat Mass Transfer* 49 2829-2839, 2006.
- [8] Moita A S, Teodori E, Moreira A L N, Karayiannis T G *et al*, Effects of surface micro-structuring on the nucleation mechanisms, IV Conf. Nacional Mecânica dos Fluidos, Termodinâmica e Energia – MEFTE, Lisbon, Portugal, 2012.
- [9] Karayiannis T G *et al*, Steps towards the development of an experimentally verified simulation of pool nucleate boiling on a silicon wafer with artificial sites, *Applied Thermal Engineerig*, 29 1327-1337, 2009.
- [10] Chaptun S, Watanabe M, Shoji M, Nucleation site interaction in pool nucleate boiling on a heated surface with triple artificila cavities, *International journal of Heat and Mass Transfer* 47 (2004) 3583-3587.